Correlating Traveling-Wave Arrival Times to the Bewley Diagram—A New Systematic Approach for Offline Traveling-Wave Fault Locating

Stephen Marx, *Bonneville Power Administration*
Ellery Blood and Greg Smelich, *Schweitzer Engineering Laboratories, Inc.*

Abstract—Traveling-wave-based fault-locating (TWFL) methods have become widely popular in fault locators—including those available in transmission line protective relays—because of their improved accuracy over impedance-based methods. The Bewley diagram offers a time-space representation that shows how traveling waves (TWs) traverse along a transmission line following a disturbance, such as a fault. The Bewley diagram is commonly used to visualize, confirm, or fine-tune TWFL results provided by the fault locator. It also allows for determining alternative fault-location hypotheses or obtaining TWFL results offline when they are not provided automatically by the fault locator. Until recently, Bewley diagram-based analysis software provided TWFL results by making use of, at most, three parameters and three TW arrival times to provide correlation between the Bewley diagram and TW signals captured by ultra-high-resolution event records. These parameters are the fault initiation time (t_0), the TW line propagation time (*TWLPT*), and the per-unit fault location (*m*). To improve the accuracy of the calculated fault location, we can now obtain a more precise correlation between the Bewley diagram and the recorded TW arrival times by including a fourth TW arrival time and a fourth parameter, a skew factor (Δ), that compensates for various time-alignment issues between the terminals at each end of the line.

This paper introduces a systematic notation and matrix representation of the equations that determine the expected TW arrival times by using as many as four parameters: t_0, *TWLPT*, *m*, and Δ. We describe a flexible method that uses the matrix representation, and using real-world events, show how software that employs these equations improves TWFL accuracy.

I. INTRODUCTION

With the release of transmission line protective relays that include MHz-rate data acquisition and traveling-wave-based fault-locating (TWFL) technology in 2012, applications supporting the analysis of power system faults began including features to facilitate the analysis of traveling-wave (TW) data. In this paper, we explore the equations that determine the expected arrival times of TWs at a line terminal and describe the evolution of software-based TWFL methods.

In Section II, we review the basics of TWFL technology. We define a systematic, matrix-based method and associated notation for representing the TW arrival times and describe how these expressions are used to derive the general TWFL equations.

In Section III, we explain how the Bewley diagram helps to better understand the relationship between the numerous TW arrival times, the fault location, and the parameters that govern the TW arrival times. This paper describes the contribution of four parameters that define the TW arrival times at each line terminal (t_0, *TWLPT*, *m*, and Δ) and provides a new systematic approach for offline TWFL that uses as many as four TW arrival times—identified from ultra-high-resolution event records—to simultaneously solve a system of equations for all four parameters. This method provides improved flexibility in performing TWFL and improved accuracy over existing Bewley-based methods used for offline analysis. We further explore potential sources of error in the TWFL methods and introduce compensation techniques that may be applied.

We also describe a TWFL software tool based on the Bewley diagram that includes these compensation methods and how they are employed. Using this tool, the operator selects which TW arrival times factor into the solution, providing greater flexibility for the operator to fully explore the effect of the different parameters.

Finally, in Section IV, we review event records from several real-world faults and show how applying this Bewley diagram tool—which has recently been implemented in event analysis software—improves the accuracy of the results obtained from the new offline TWFL method. We compare the accuracy and flexibility of the new method to the traditional single- and double-ended TWFL methods that use two TW arrival times and two parameters to calculate the fault location. Similarly, we compare the new method to TWFL methods that use three TW arrival times and three parameters to calculate the fault location.

II. REVIEW OF TRAVELING-WAVE-BASED FAULT LOCATING

A. TWs and the Bewley Diagram

TWs are launched by the voltage step change that occurs when a disturbance, such as a fault, occurs on a line. The size of the step change, and therefore the size of the TWs, is affected by several factors, including the characteristic impedance of the line (which is a function of the distributed inductance and capacitance), the point on the voltage waveform when the disturbance occurred, and fault resistance. When a fault occurs, the voltage step change creates both current and voltage TWs that travel from the fault toward each line terminal and arrive at each end after some period of time. The initial current and voltage TWs have the same polarity and are related in magnitude by the characteristic impedance of the line. When these initial TWs arrive at each line terminal, the current TW becomes inverted because of the orientation of the CTs [1].

As explained in [2], when an incident TW arrives at a termination point (i.e., a change in the characteristic impedance, such as a line terminal or the fault), some of the energy continues in the same direction (a transmitted TW) and some of the energy reflects in the opposite direction (a reflected TW). The size of each transmitted and reflected TW—as well as the polarity of the reflected TW—depends on the size of the incident TW and the characteristic impedance on either side of the termination point.

TWs move at approximately 98 percent of the speed of light ($0.98c$) on overhead lines and at approximately 45 to 85 percent of the speed of light ($0.45c$ to $0.85c$) on underground cables [3]. The TW line propagation velocity, PV, is determined by the distributed inductance and capacitance of the line and is equal to the line length, LL, divided by the TW line propagation time, $TWLPT$, i.e., $PV = LL / TWLPT$. $TWLPT$ is the one-way end-to-end travel time of a TW on the line and is a setting required by some TW-based fault locators. Other TW-based fault locators use PV expressed as a per-unit value of the speed of light, $LPVEL$, i.e., $LPVEL = PV / c$.

In the 1930s, L. V. Bewley developed a reflection lattice diagram that would later be named after him [4] [5]. The Bewley diagram allows us to visualize and predict TW arrival times at each terminal based on the line configuration, fault location, and fault initiation time. The diagram further shows the interactions between a variety of reflection points, allowing the operator to make sense of the numerous TW arrivals that may be visible in the TW signals captured by a recording device.

Fig. 1 shows a Bewley diagram for a homogeneous two-terminal line, representing TWs as they travel after being launched by a fault at the fault initiation time, t_0, located a per-unit distance, m, from the local terminal, L, and $1 - m$ from the remote terminal, R. The TWs progress along the vertical time axis (time increases from top to bottom) and simultaneously progress horizontally along the distance axis.

B. Systematic Notation and Matrix Representation of TW Arrival times

Fig. 1 also shows TWs that arrive at each terminal following a variety of time-spatial paths. The paths can include being reflected from the fault point, being transmitted through the fault point, being reflected from the opposite terminal, or a combination of these paths. The arrival of each TW at Terminal L or Terminal R corresponds to the respective time stamp, where the order of the subscripts in the time stamp label represents the order the initial TW and subsequent reflections were observed at the two terminals. For example, t_{LR} is the arrival time of a TW that first arrived at Terminal L, reflected off Terminal L, transmitted through the fault, and was finally observed at Terminal R. Although additional TW arrivals may be visible on recorded data, only the TW arrivals up to and including those with labels having three subscripts are included in Fig. 1 because TWs typically attenuate below the noise threshold by this point.
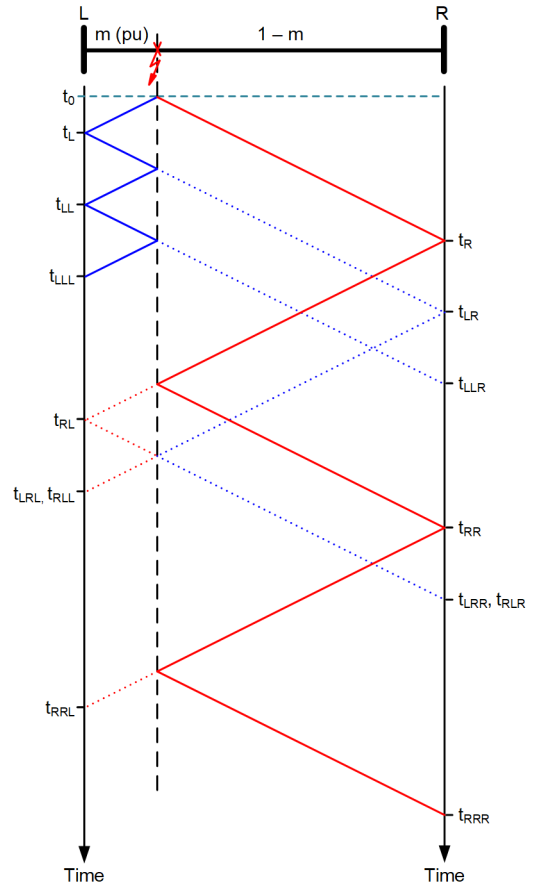

Fig. 1.   Bewley diagram showing systematic naming of TW arrival times.

This systematic notation allows unambiguous calculation of the TW arrival times by relating them to the Bewley lattice parameters $TWLPT$, t_0, and m. Because $TWLPT$ is the amount of time it takes a TW to traverse the entire line, $m \cdot TWLPT$ is the amount of time it takes a TW to travel from the fault to Terminal L. The first TW arrival time at Terminal L is t_L, which therefore occurs at $m \cdot TWLPT$ after t_0, as shown in (1a). This can also be shown in the matrix form of $Ax = t$ as (1b), where x is the vector of Bewley lattice parameters and t is the vector of TW arrival times. A is the TW alignment matrix that we use to translate the parameters to arrival times.

$$t_L = t_0 + m \cdot TWLPT \tag{1a}$$

$$\begin{bmatrix} 1 & 1 & 0 \end{bmatrix} \begin{bmatrix} t_0 \\ m \cdot TWLPT \\ TWLPT \end{bmatrix} = \begin{bmatrix} t_L \end{bmatrix} \tag{1b}$$

The first TW that arrives at Terminal L after being reflected from the fault arrives at t_{LL}, which is $3 \cdot m \cdot TWLPT$ after t_0, as shown in (2a). This can also be shown in matrix form as (2b).

$$t_{LL} = t_0 + 3 \cdot m \cdot TWLPT \tag{2a}$$

$$\begin{bmatrix} 1 & 3 & 0 \end{bmatrix} \begin{bmatrix} t_0 \\ m \cdot TWLPT \\ TWLPT \end{bmatrix} = \begin{bmatrix} t_{LL} \end{bmatrix} \tag{2b}$$

Similarly, $(1 - m) \cdot TWLPT$ is the amount of time it takes a TW to travel from the fault to Terminal R. The first TW arrival time at Terminal R is t_R, which therefore occurs at $(1 - m) \cdot TWLPT$ after t_0, as shown in (3a) and (3b).

$$t_R = t_0 + (1 - m) \cdot TWLPT \tag{3a}$$

$$\begin{bmatrix} 1 & -1 & 1 \end{bmatrix} \begin{bmatrix} t_0 \\ m \cdot TWLPT \\ TWLPT \end{bmatrix} = [t_R] \tag{3b}$$

Subsequent TW arrival times are calculated by the addition of time as follows:

1. A reflection from Terminal L, reflecting off the fault, then arriving back at Terminal L adds $2 \cdot m \cdot TWLPT$ or [0 2 0] to the applicable row of the A matrix.
2. A reflection from Terminal R, reflecting off the fault, then arriving back at Terminal R adds $2 \cdot (1 - m) \cdot TWLPT$ or [0 –2 2] to the applicable row of the A matrix.
3. A reflection from one terminal, transmitting through the fault, and arriving at the other terminal adds $TWLPT$ or [0 0 1] to the applicable row of the A matrix.

Using this system, the path a TW traverses is uniquely described by the subscripts of the TW arrival time labels. The TW arrival times shown in Fig. 1 are shown in (4a) for Terminal L and (4b) for Terminal R. As shown in Fig. 1, only the rows up to and including three subscripts of the TW arrival time label are shown in (4a) and (4b).

$$\begin{bmatrix} 1 & 1 & 0 \\ 1 & 3 & 0 \\ 1 & 5 & 0 \\ 1 & -1 & 2 \\ 1 & -3 & 4 \\ 1 & 1 & 2 \\ 1 & 1 & 2 \end{bmatrix} \begin{bmatrix} t_0 \\ m \cdot TWLPT \\ TWLPT \end{bmatrix} = \begin{bmatrix} t_L \\ t_{LL} \\ t_{LLL} \\ t_{RL} \\ t_{RRL} \\ t_{RLL} \\ t_{LRL} \end{bmatrix} \tag{4a}$$

$$\begin{bmatrix} 1 & -1 & 1 \\ 1 & -3 & 3 \\ 1 & -5 & 5 \\ 1 & 1 & 1 \\ 1 & 3 & 1 \\ 1 & -1 & 3 \\ 1 & -1 & 3 \end{bmatrix} \begin{bmatrix} t_0 \\ m \cdot TWLPT \\ TWLPT \end{bmatrix} = \begin{bmatrix} t_R \\ t_{RR} \\ t_{RRR} \\ t_{LR} \\ t_{LLR} \\ t_{LRR} \\ t_{RLR} \end{bmatrix} \tag{4b}$$

To better understand the offline TWFL method proposed in this paper, it is helpful to first review the methods already implemented in existing protective relays and fault locators, which use two TW arrival times to estimate the fault location. Section II.C explains how the double-ended TWFL (DETWFL) method may be used to estimate the fault location by using t_L and t_R in Fig. 1, which are the arrival times of the initial TW at Terminals L and R, respectively. Similarly, Section II.D explains how the single-ended TWFL (SETWFL) method may be used to estimate the fault location by using t_L and t_{LL} in Fig. 1, which are the arrival times of the initial TW at Terminal L and the first reflection from the fault, respectively. Section III then expands on these methods and explains a new systematic approach for offline TWFL that can provide improved accuracy of results by using up to four TW arrival

times and by allowing flexibility for which TW arrival times are selected.

C. Double-Ended TW-Based Fault Locating by Using Two TW Arrival Times

Fig. 2 is a simplified version of Fig. 1 that shows the initial TWs arriving at Terminal L and Terminal R at times t_L and t_R, respectively. Expressions representing the arrival times are given in (1b) and (3b), and (5) combines them in a single matrix expression. Equation (5) is equivalent to combining the t_L row from (4a) and the t_R row from (4b) into a single expression. If we declare $TWLPT$ as constant and focus on columns 1 and 2 of the A matrix in (5), we see it is full rank (i.e., the rows are linearly independent and thus invertible as indicated by a nonzero determinant [6]), and therefore, the equation can be arranged to solve for t_0 and $m \cdot TWLPT$ as in (6). This process provides sufficient information to draw the Bewley lattice diagram shown in Fig. 2.
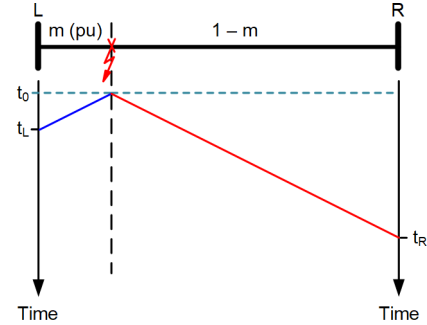

Fig. 2. First TW arrival times at Terminals L (t_L) and R (t_R).

$$\begin{bmatrix} 1 & 1 & 0 \\ 1 & -1 & 1 \end{bmatrix} \begin{bmatrix} t_0 \\ m \cdot TWLPT \\ TWLPT \end{bmatrix} = \begin{bmatrix} t_L \\ t_R \end{bmatrix} \tag{5}$$

$$\begin{bmatrix} t_0 \\ m \cdot TWLPT \end{bmatrix} = \frac{1}{2} \begin{bmatrix} t_L + t_R - TWLPT \\ t_L - t_R + TWLPT \end{bmatrix} \tag{6}$$

The second (bottom) row of (6) can be arranged to isolate m, thus solving for the per-unit fault location (7). The details of the derivation of (6) and (7) are available in Appendix A. Because t_0 cannot be directly measured by the devices located at each line terminal, (7) is commonly derived by rearranging (1a) and (3a) to solve for t_0, setting them equal to each other, and solving for m. Notice that (7) relies on both t_L and t_R, but it does not require t_0. Equation (7) is the general equation (in per-unit) used for the DETWFL method. Multiplying (7) by LL (in units of length, typically km or mi), as shown in (8), converts the per-unit fault location (lower case m) into a fault location in units of km or mi (capital M) [1] [2] [7] [8].

$$m = \frac{1}{2}\left(1 + \frac{t_L - t_R}{TWLPT}\right) \tag{7}$$

$$M = m \cdot LL \tag{8}$$

Because this method relies on t_L and t_R, device-to-device communications are required to exchange data needed to determine the TW arrival time at each terminal. Alternatively, an offline method, such as the one described in [8] or the one

described in Section III of this paper may be applied. Furthermore, the devices must be synchronized to a common time reference.

D. Single-Ended TW-Based Fault Locating by Using Two TW Arrival Times

Fig. 3 is a simplified version of Fig. 1 that shows the initial TW and the first reflection from the fault that arrive at Terminal L at time t_L and t_{LL}, respectively. Expressions representing the arrival times are given in (1b) and (2b), and (9) combines them in a single matrix expression. Equation (9) is equivalent to combining the t_L and t_{LL} rows from (4a) into a single expression. If we declare *TWLPT* as constant and focus on columns 1 and 2 of the *A* matrix in (9), we see it is full rank, and thus, the equation can be arranged to solve for t_0 and $m \cdot TWLPT$ as in (10).
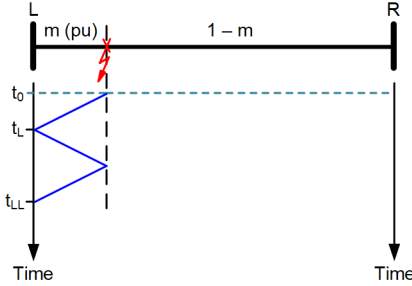

Fig. 3.   First (t_L) and second (t_{LL}) TW arrival times at Terminal L.

$$\begin{bmatrix} 1 & 1 & 0 \\ 1 & 3 & 0 \end{bmatrix} \begin{bmatrix} t_0 \\ m \cdot TWLPT \\ TWLPT \end{bmatrix} = \begin{bmatrix} t_L \\ t_{LL} \end{bmatrix} \qquad (9)$$

$$\begin{bmatrix} t_0 \\ m \cdot TWLPT \end{bmatrix} = \frac{1}{2} \begin{bmatrix} 3t_L - t_{LL} \\ -t_L + t_{LL} \end{bmatrix} \qquad (10)$$

The second (bottom) row of (10) can be arranged to isolate *m*, thus solving for the per-unit fault location (11). The details of the derivation of (10) and (11) are available in Appendix A. Equation (11) is the general equation (in per-unit) used for the SETWFL method [1] [2]; it is commonly derived by subtracting (1a) from (2a) and solving for *m*. Because the SETWFL method relies only on data from the local device, this method does not require device-to-device communications nor synchronizing to an absolute time reference.

$$m = \left(\frac{1}{2}\right) \cdot \left(\frac{t_{LL} - t_L}{TWLPT}\right) \qquad (11)$$

As explained previously, the SETWFL method relies on identifying the first TW reflected from the fault. However, it may be challenging to distinguish this TW from other reflected TWs that may arrive at the terminal. One such case is depicted in Fig. 4a, which shows a fault located at a distance of *m* from Terminal L. The fault produces an initial TW and first reflection from the fault that arrive at Terminal L with the arrival time difference of Δt_a, calculated in (12). This value is the same as Δt_b in Fig. 4b, which is the arrival time difference between the initial TW and first reflection from Terminal R for a fault located at a distance of $(1 - m)$ from Terminal L (a distance of *m* from Terminal R), as calculated in (13). To

remove this ambiguity, additional logic, such as that described in [2], may be applied to the SETWFL algorithm to distinguish a fault at *m* from a fault at $1 - m$. Similarly, the method explained in this paper may be applied to distinguish between the two fault locations by using a Bewley diagram in conjunction with a transient record captured at Terminal L to correlate the arrival of up to three TWs.
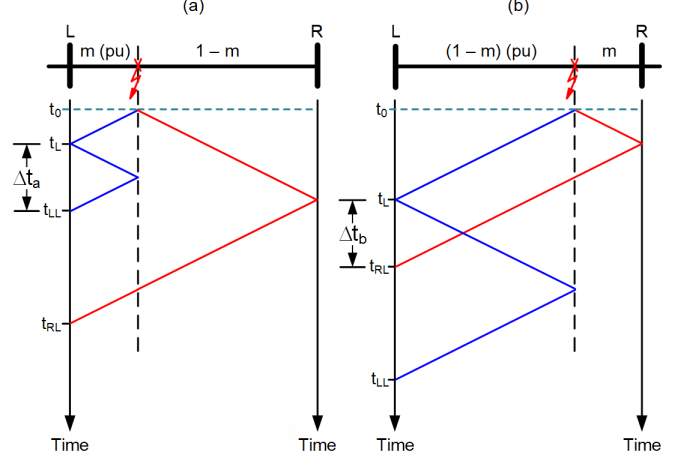

Fig. 4.   Example of fault-location ambiguity for the SETWFL method.

$$\Delta t_a = t_{LL} - t_L$$
$$= ([1 \quad 3 \quad 0] - [1 \quad 1 \quad 0]) \begin{bmatrix} t_0 \\ m \cdot TWLPT \\ TWLPT \end{bmatrix}$$
$$= [0 \quad 2 \quad 0] \begin{bmatrix} t_0 \\ m \cdot TWLPT \\ TWLPT \end{bmatrix} \qquad (12)$$
$$= 2m \cdot TWLPT$$

$$\Delta t_b = t_{RL} - t_L$$
$$= ([1 \quad 1 \quad 1] - [1 \quad -1 \quad 1]) \begin{bmatrix} t_0 \\ m \cdot TWLPT \\ TWLPT \end{bmatrix}$$
$$= [0 \quad 2 \quad 0] \begin{bmatrix} t_0 \\ m \cdot TWLPT \\ TWLPT \end{bmatrix} \qquad (13)$$
$$= 2m \cdot TWLPT$$

E. Availability of Results and Error Considerations

Transmission line protective relays and fault locators that use the DETWFL or SETWFL method provide an estimate of the fault location only if the supervisory conditions have been satisfied and the device was able to identify the required TW arrival times. Therefore, TWFL results may not be automatically available in some cases, such as when time-synchronization or device-to-device communications is not available in applications that use the DETWFL method or if the fault locator was not triggered.

When TWFL results are not automatically provided, an offline method may be used to manually obtain them. Reference [8] describes an offline approach to estimate the fault location by using the DETWFL method when relay-to-relay communications are not available. This method uses the capability of ultra-high-speed (UHS) line relays that measure

and record power system signals at 1 Msps and provide TW arrival time data in IEEE COMTRADE transient records. The offline DETWFL method described in [8] uses two TW arrival times (t_L and t_R) to calculate the fault location by using (7) and (8). Similarly, the offline method described in this paper for the SETWFL and DETWFL methods may be applied to estimate the fault location by using transient records and the Bewley diagram, as demonstrated by the real-world event analysis examples in Section IV.

The TWFL methods rely on user-provided settings for LL and $TWLPT$. Optionally, the DETWFL method also relies on user-provided settings for the TW cable propagation time ($TWCPT$) at each terminal (see Section III.D for more information about the $TWCPT$ setting). As explained in [7], accuracy of the line data impacts TWFL accuracy. For example, 1 percent of error in the LL setting results in 1 percent of error in the fault location, and 1 µs of error in the $TWLPT$ setting results in a TWFL error of as much as 500 ft (150 m) for overhead lines and as much as 250 ft (75 m) for underground cables. Reference [7] explains why there is ambiguity in the line length by depicting four different definitions of distance between two adjacent towers. It also provides suggestions on how to improve the accuracy of the LL, $TWLPT$, and $TWCPT$ settings. In addition to errors in device settings for the line data, [7] explains that 0.1 µs of error in device time stamping results in a TWFL error of about 50 ft (15 m) for overhead lines and about 25 ft (7.5 m) for underground cables. As shown in the examples in Section IV, the offline method described in this paper may be used to fine-tune results that were automatically provided if they are suspected to be inaccurate because of errors in the LL, $TWLPT$, or $TWCPT$ settings or errors in the measured TW arrival times.

III. BEWLEY DIAGRAM SOFTWARE APPLICATION FOR TW-BASED FAULT LOCATING

A. Background of the Bewley Diagram Application

In 2014, a Bewley Diagram application was added to event analysis software [9] with movable cursors attached to the lattice reflection points that are associated with the arrival of TWs at each terminal. When describing the Bewley Diagram application, the notation for TW arrival times is synonymous with the cursor associated with that TW arrival. By moving the two cursors used in (7) or (11), an operator can dynamically align lattice reflection points to features of the recorded waveform and visualize how adjustments to the lattice affect the t_0 and m parameters. Development of the Bewley Diagram application as a tool for event analysis significantly advanced the state of the art for TWFL.

B. Original Bewley Diagram Application

In addition to the TWFL techniques described in Section II, the Bewley Diagram application used for TWFL introduced the ability to move the three cursors whose labels are referenced in (14a) and (14b) to dynamically align lattice reflection points, along with the additional flexibility of adjusting $TWLPT$, and immediately see the correlation between Bewley lattice reflection points and TWs observed in the recorded signals.

We can measure $TWLPT$ directly by analyzing a line energization event or calculate it using LL and PV. This value for $TWLPT$ is then integrated into the TWFL device settings as a constant. The actual value of $TWLPT$, however, is not constant but is dependent on a variety of factors including line sag, air temperature, humidity, etc. [7] [10]. The results from any TWFL algorithm can therefore contain error if it does not account for $TWLPT$ variability, as described in Section II.E.

The original Bewley Diagram application displays up to three cursors that the operator may align to various TW arrival times. The initial two-cursor alignment provides fault locating based on (7) for DETWFL and (11) for SETWFL. For DETWFL, cursors are aligned to t_L and t_R. For SETWFL, cursors are aligned to t_L and t_{LL}. A third cursor is made available for the operator to align to an additional TW arrival time. For DETWFL, the third cursor is aligned with t_{LL}. For SETWFL, the third cursor is aligned to t_{RL}. The resulting systems of linear equations to be solved are shown in (14a) for DETWFL and (14b) for SETWFL. Note that in this version of the Bewley Diagram application, the first two cursors only adjust fault location and the third cursor moves along with the adjustments of the lattice. To adjust $TWLPT$, the operator adjusts the third cursor while the software holds the first two cursors constant, simultaneously solving for all three parameters.

$$\begin{bmatrix} 1 & 1 & 0 \\ 1 & -1 & 1 \\ 1 & 3 & 0 \end{bmatrix} \begin{bmatrix} t_0 \\ m \cdot TWLPT \\ TWLPT \end{bmatrix} = \begin{bmatrix} t_L \\ t_R \\ t_{LL} \end{bmatrix} \tag{14a}$$

$$\begin{bmatrix} 1 & 1 & 0 \\ 1 & 3 & 0 \\ 1 & -1 & 2 \end{bmatrix} \begin{bmatrix} t_0 \\ m \cdot TWLPT \\ TWLPT \end{bmatrix} = \begin{bmatrix} t_L \\ t_{LL} \\ t_{RL} \end{bmatrix} \tag{14b}$$

In early 2022, the state of the art for TWFL saw additional improvements. Two key advancements were introduced based on field experience to improve accuracy and usability: 1) flexibility in selecting and pinning cursors and 2) accounting for time skew. These improvements are described in Section III.C and Section III.D, respectively.

C. New Bewley Diagram Application—Selecting and Pinning Three Cursors to Refine Fault Location and TWLPT

The first key advancement was extending the power of the Bewley Diagram application by allowing the manipulation of the lattice at more than just the three TW arrival times described in (14a) and (14b).

By leveraging the systematic definition of TW arrival times on the lattice, as described in Section II.B, the operator can now select cursors for any point where the TWs arrived at Terminal L and Terminal R, as shown and labeled in Fig. 1. The definitions of the time stamps associated with each of these labeled cursors are shown in (4a) for TWs that arrive at Terminal L and (4b) for TWs that arrive at Terminal R. Note that $t_{LRR} = t_{RLR}$ and $t_{LRL} = t_{RRL}$.

Using this updated design, the operator can manipulate any three cursors to dynamically recalculate $TWLPT$ and the fault location. To help the operator specify which cursors should be held constant and thus which rows of (4a) and (4b) contribute

to the solution, a pinning paradigm was introduced. If a cursor is pinned, its position remains constant, effectively fixing that point of the lattice in place. Depending on the number of cursors pinned, a subset of the combined matrix equations of (4a) and (4b) are solved; first solving t_0, then $m \cdot TWLPT$, and then $TWLPT$ as the number of pinned cursors increases. See Appendix B for details on the underlying math.

The TWFL process that uses the Bewley Diagram application now enables an operator to use the pinning paradigm to add additional parameters to the solution space as necessary to refine the TWFL result. When the operator manipulates a cursor and no other cursors are pinned, t_0 is solved with $m \cdot TWLPT$ and $TWLPT$ as constants. The system of equations represents a configuration with one equation and one unknown. That is, t_0 is the single degree of freedom. All the other cursors move along with the lattice.

Pinning a single cursor modifies the behavior slightly. Now, when the operator manipulates another cursor, the pinned cursor remains static. This becomes a configuration with two equations and two unknowns (i.e., two degrees of freedom). The time stamps of the pinned and manipulated cursors are the inputs, and t_0 and $m \cdot TWLPT$ are the outputs.

Having two cursors pinned and manipulating a third is a configuration with three equations and three unknowns (i.e., three degrees of freedom). The time stamps of the pinned and manipulated cursors are the inputs, and t_0, $m \cdot TWLPT$, and $TWLPT$ are the outputs.

Unlike the original Bewley Diagram application, where only the cursors whose labels are referenced in (14a) and (14b) were selectable, the new Bewley Diagram application allows the operator to select from any of the TW arrival times shown in Fig. 1 and described by (4a) and (4b). The ability to select alternate TW arrivals is beneficial and may be necessary because of distorted waveforms and certain fault locations, including but not limited to fault locations and system configurations that result in multiple TW arrivals coinciding. The superposition of currents from multiple coincident TW arrivals can severely distort the shape of the TW, making identification of the arrival time infeasible. In this situation, an alternate TW arrival that does not suffer this overlap may be selected.

Additionally, improved accuracy may be achieved by selecting a later TW arrival time, which tends to average out the timing uncertainty. When calculating the fault location, the expression that represents the difference in time stamps will tend to include multiples of the m and $TWLPT$ parameters. For example, for SETWFL, $t_{LL} - t_L$ is $2 \cdot m \cdot TWLPT$, whereas $t_{LLL} - t_L$ is $4 \cdot m \cdot TWLPT$. Using t_L and t_{LL} will divide the difference between the time stamps by 2, but using t_L and t_{LLL} will divide it by 4, thus potentially reducing the measurement error by a factor of 2. Similarly, using TWs that have traversed the full length of the line multiple times will tend to reduce errors associated with calculating $TWLPT$. For example, $t_{LR} - t_L$ is $TWLPT$, whereas using $t_{LRL} - t_L$ is $2 \cdot TWLPT$.

For a system where the error in the TW arrival time stamp can be modeled as additive white Gaussian noise (AWGN), we can quantify the effect of selecting different TW arrivals on our estimate of $m \cdot TWLPT$ and $TWLPT$ [11]. By performing SETWFL using t_L, t_{LLL}, and t_{LRL}, the effect of AWGN may be reduced by a factor of 2 over the original Bewley Diagram application, which exclusively used t_L, t_{LL}, and t_{RL}. However, we also know that as a TW traverses a longer path, the effects of dispersion (spreading out of the TW) and attenuation (decreasing the magnitude of the TW) are increased. Therefore, a trade off exists between using later TW arrivals that decrease the effect of measurement error yet have greater dispersion that increases the error in their arrival time.

D. New Bewley Diagram Application—Selecting and Pinning Four Cursors to Solve for Time Skew Between Stations

The second key advancement adds a fourth degree of freedom over which operators may optimize the DETWFL solution.

When a TW waveform is loaded into the Bewley Diagram application, the software checks for the $TWCPT$ setting. If found, the plotted signals are time adjusted to compensate for the time it takes a TW to travel from the instrument transformers to the terminals of the relay. So, even though the recorded data represent the arrival times of the TWs at the terminals of the recording device, the displayed data represent the arrival times of the TWs at the instrument transformers. This compensation in the recorded signals allows for improved accuracy in the fault-location estimate by accounting for the difference in cable lengths between the instrument transformers and the recording device at Terminals L and R. Thus, the DETWFL equation shown in (7) could also be written as shown in (15), where t_{Lr} and t_{Rr} represent the raw TW arrival times at the recording device without the $TWCPT$ compensation applied [7] [8]. Note that for SETWFL, all TWs that arrive at the terminal travel along the same secondary cabling, so $TWCPT$ compensation is not necessary.

$$
\begin{aligned}
m &= \frac{1}{2}\left(1 + \frac{(t_{Lr} - TWCPT_L) - (t_{Rr} - TWCPT_R)}{TWLPT}\right) \\
&= \frac{1}{2}\left(1 + \frac{(t_{Lr} - t_{Rr}) - (TWCPT_L - TWCPT_R)}{TWLPT}\right)
\end{aligned}
\tag{15}
$$

Because of the methods employed to interpolate a precise TW arrival time from the recorded TW signals, the shape of the TW may affect the interpolated TW arrival time. The shape is strongly influenced by the system and equipment configuration at the substation and may be further affected by factors such as dispersion, coinciding TW arrivals, and secondary wiring resonance. Therefore, different effects on the TW arrival time interpolation at either end are expected. Additionally, $TWCPT$ settings errors can introduce a time-stamp offset between Terminals L and R.

Equation (15) shows how the effects of the variables $TWCPT_L$ and $TWCPT_R$ can be grouped together into a combined term. This can also be applied to the wave shape issue described in the previous paragraph, differences in instrument transformer group delay, and other factors local to one terminal or the other. Because the relative (i.e., not absolute) TW arrival times are important for DETWFL, we can collect all the time-

stamp offset factors into a single variable representing the relative time skew between stations (Δ). To incorporate Δ, we append it as a fourth element of the Bewley parameter vector (x) and add a fourth column to the TW alignment matrix (A), as shown in (16a) and (16b). Because the skew is relative between stations, we can apply it to the Terminal R equations. This results in column 4 of A for Terminal R being all 1s and for Terminal L being all 0s. An alternative implementation could distribute the skew evenly between the two terminals by using 0.5 for Terminal R and –0.5 for Terminal L. Incorporating a fourth TW arrival time enables solving the system of equations for Δ. Additionally, because Δ applies to the time skew between two terminals, it only applies to the DETWFL method.

$$\begin{bmatrix} 1 & 1 & 0 & 0 \\ 1 & 3 & 0 & 0 \\ 1 & 5 & 0 & 0 \\ 1 & -1 & 2 & 0 \\ 1 & -3 & 4 & 0 \\ 1 & 1 & 2 & 0 \\ 1 & 1 & 2 & 0 \end{bmatrix} \begin{bmatrix} t_0 \\ m \cdot TWLPT \\ TWLPT \\ \Delta \end{bmatrix} = \begin{bmatrix} t_L \\ t_{LL} \\ t_{LLL} \\ t_{RL} \\ t_{RRL} \\ t_{RLL} \\ t_{LRL} \end{bmatrix} \quad (16a)$$

$$\begin{bmatrix} 1 & -1 & 1 & 1 \\ 1 & -3 & 3 & 1 \\ 1 & -5 & 5 & 1 \\ 1 & 1 & 1 & 1 \\ 1 & 3 & 1 & 1 \\ 1 & -1 & 3 & 1 \\ 1 & -1 & 3 & 1 \end{bmatrix} \begin{bmatrix} t_0 \\ m \cdot TWLPT \\ TWLPT \\ \Delta \end{bmatrix} = \begin{bmatrix} t_R \\ t_{RR} \\ t_{RRR} \\ t_{LR} \\ t_{LLR} \\ t_{LRR} \\ t_{RLR} \end{bmatrix} \quad (16b)$$

Building on the previous discussion about cursor behavior, when we have three cursors pinned and are manipulating a fourth, we have a configuration with four equations and four unknowns, (i.e., four degrees of freedom). The time stamps of the pinned and manipulated cursors are the inputs, and t_0, $m \cdot TWLPT$, $TWLPT$, and Δ are the outputs. See Appendix B for details on the underlying math.

IV. ANALYSIS OF REAL-WORLD EVENTS

This section uses 1 Msps event records captured in the field to demonstrate the systematic approach of TWFL described in this paper. The event records were captured by UHS line relays installed to monitor a two-terminal 161 kV, 73 mi (117 km) line. The UHS relays at the local (L) and remote (R) terminals are time-synchronized to an absolute reference by using GPS clocks. Event analysis software that includes the Bewley Diagram application [9] enables the user to open event records and plot the 1 Msps current and voltage signals. The software also allows the user to obtain the phase TWs and modal TWs (zero, alpha, and beta Clarke components) for manual analysis and apply time cursors that replicate the interpolation method

used by UHS relays to obtain TW arrival times with submicrosecond accuracy [2]. If the *TWCPT* values are available in the device settings, the Bewley Diagram application compensates the time stamps of the TW signals to remove the delay associated with the secondary cables.

It should be noted that the line is terminated with only a power transformer at Terminal R. Therefore, any current TW arriving at that terminal is reflected with opposite polarity. For this reason, the current TW that reflects off Terminal R and arrives at Terminal L at time t_{RL} has the same polarity as the current TWs that arrive at times t_L and t_{LL}. This relationship is important for correctly interpreting the measured signals at Terminal L, shown in the examples in this section. Additionally, if only a power transformer terminates the line, this configuration reduces the ability of a recording device to dependably measure and accurately time-stamp TWs when they arrive at that terminal. For the example in Section IV.B, the effect of the transformer caused the arrival time of the initial TW at Terminal R to not be identified by the UHS relay, making the automatic calculation of DETWFL results by the relays unavailable. Reference [3] provides additional details about how characteristic impedances affect the dependability and accuracy of TWFL.

A. Improved Accuracy of SETWFL Results

The example in this section shows how improved accuracy of the SETWFL method is achieved by using the Bewley Diagram application in conjunction with three TW arrival times identified in the event records. This example demonstrates the ability to pin selected cursors in the Bewley Diagram application, which allows the operator to choose TW time stamps with high confidence. Once the operator selects and pins the cursors, the software sets the time stamps as constants and solves the system of equations for t_0, $m \cdot TWLPT$, and $TWLPT$, as explained in Section III.C. If the cursors are not pinned, they may move when line parameters or other time cursors are modified, which could result in degraded alignment between the Bewley diagram and the observed TW signals or cause unintentional modification of the Bewley diagram during analysis. Furthermore, this example demonstrates the ability to choose from any of the TWs that arrived at the terminal when calculating the fault location. The ability to choose may be beneficial when some TW peaks are distorted, such as when two or more reflected TWs arrive at the terminal at the same time.

On March 22, 2022, a C-phase-to-ground fault occurred on the monitored line 27.985 mi (45.037 km) from Terminal L. Fig. 5 shows the voltage and current signals captured by the UHS relay at this terminal.
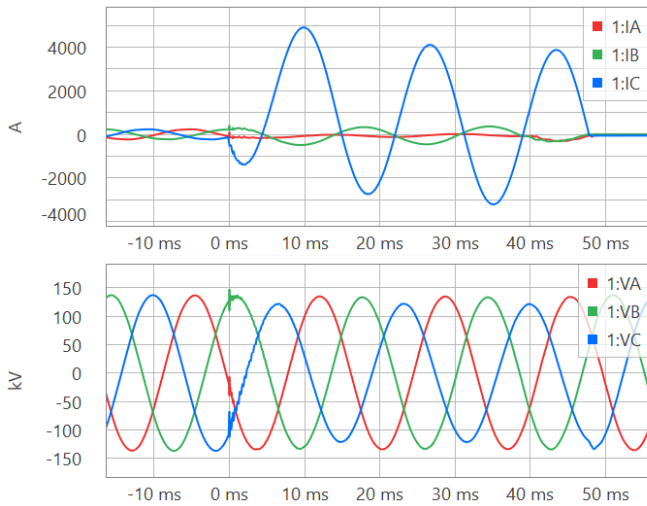
Fig. 5. Currents and voltages captured by a UHS relay at Terminal L for a C-phase-to-ground fault.

Fig. 6 shows the C-phase alpha-mode current TWs for this fault in the Bewley Diagram application with two cursors pinned that correspond to t_L and t_{LL} in Fig. 1. As explained in Appendix B, using two time cursors allows the system of equations to solve for t_0 and m by using (10). Using m in (8) provides the calculated fault location of 28.234 mi (45.438 km), which matches the SETWFL result provided by the UHS relay. The calculated result differs from the location reported by the line crew by 0.249 mi (1,315 ft; 401 m). Fig. 6 also shows that
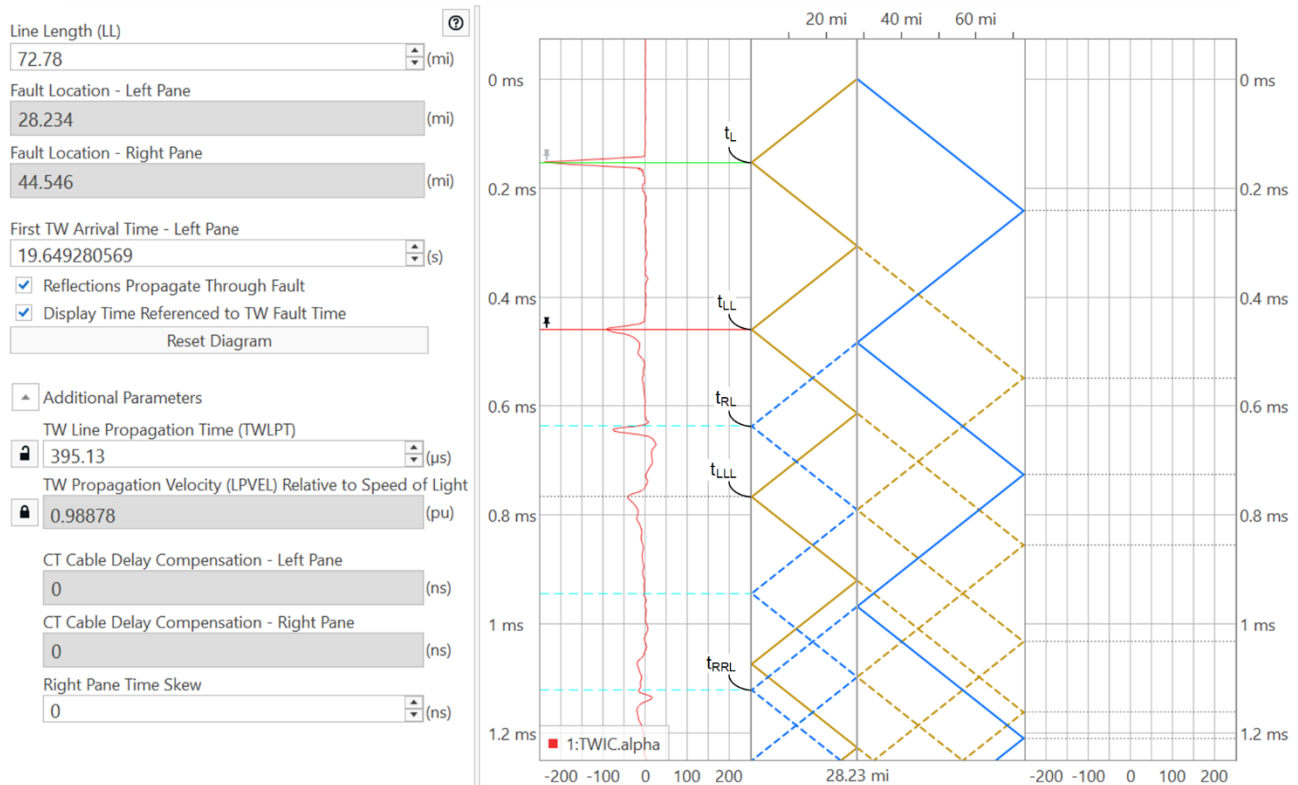
time cursors corresponding to the arrival of subsequent TWs at Terminal L (e.g., t_{RL}, t_{LLL}, and t_{RRL}) do not align well with the visible peaks in the TW signal.

In Fig. 7, a third time cursor that corresponds to t_{RL} is first aligned with the respective TW peak, and then pinned in place. As explained in Appendix B, including a third time cursor allows the system of equations to calculate a new *TWLPT* value (in this case, modifying the value from 395.13 μs to 398.63 μs) along with t_0 and m. The new calculated fault location is 27.987 mi (45.041 km), which differs from the fault location reported by the line crew by 0.002 mi (11 ft; 3 m). Fig. 7 also shows that time cursors corresponding to subsequent TWs arriving at Terminal L are better aligned with the visible peaks in the TW signal. With these refined parameters and improved results, the operator may choose to modify the *TWLPT* setting used by the fault locator.

In Fig. 7, the TWs that arrived at t_{LL} and t_{RL} have distinguished peaks and are easily identified. However, there may be cases where one or both of these TWs may be distorted because of other TWs that arrive at or near the same time. When cursors cannot be aligned with these TWs with high confidence, the user may select other TWs that are more clearly defined in the measured signal. For example, Fig. 8 shows that the TWs that arrived at time t_{LLL} and t_{RRL} (instead of t_L and t_{RL}) provide a calculated fault location of 28.005 mi (45.070 km), which differs from the fault location provided by the line crew by 0.020 mi (106 ft; 32 m).
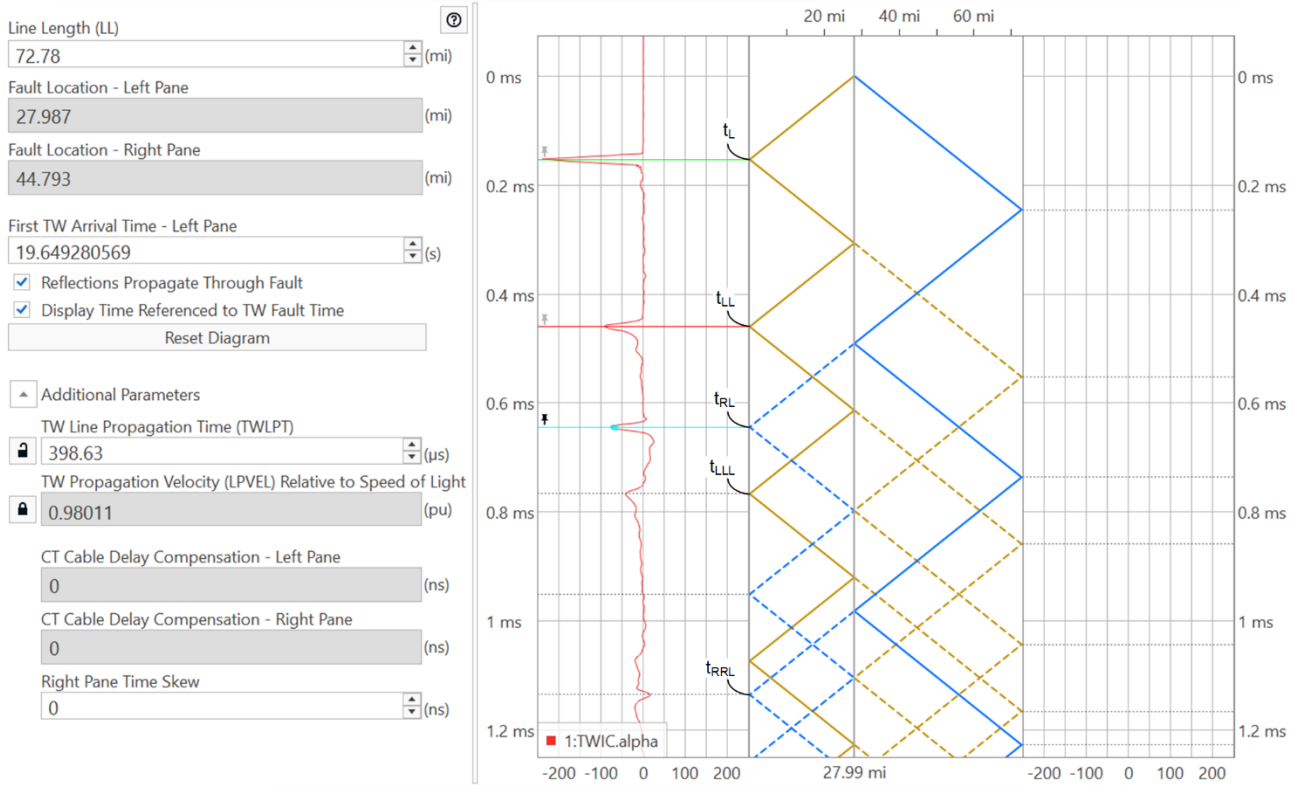

Fig. 6. Bewley diagram and SETWFL results obtained by using two TW arrivals (t_L and t_{LL}) to estimate the fault location.

Fig. 7.   Bewley diagram and SETWFL results obtained by using a third TW arrival (t_{RL}) to refine *TWLPT* for improved faut-locating accuracy.
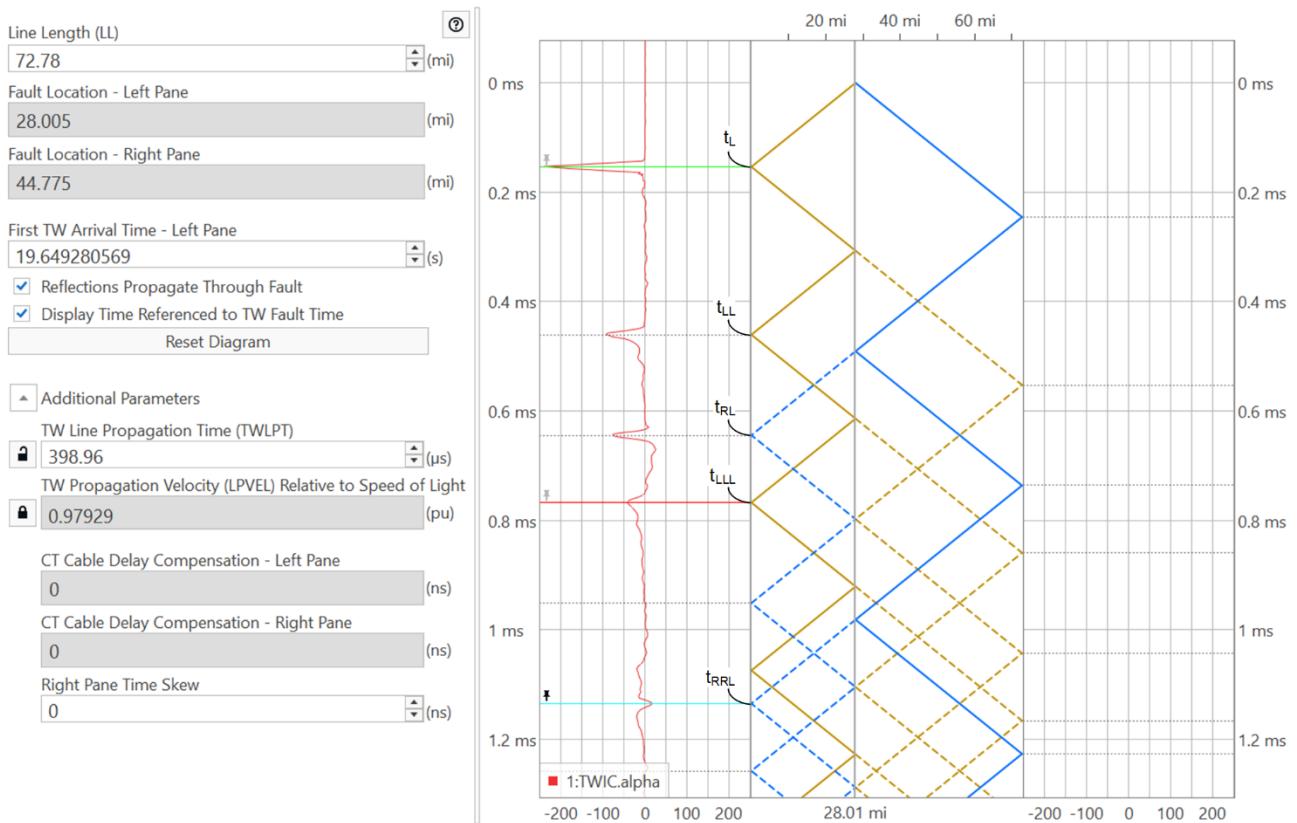

Fig. 8.   Bewley diagram and SETWFL results obtained by using t_L and alternative TW arrivals of t_{LLL} and t_{RRL}.

B.   Improved Accuracy of DETWFL Results

The example in this section compares the improved accuracy of results obtained from the DETWFL method when applying two, three, and four cursors by using the systematic approach described in Section III.

On September 19, 2020, a C-phase-to-ground fault occurred on the line 34.601 mi (55.685 km) from Terminal L. The

C-phase alpha-mode current TWs recorded at Terminal L and Terminal R are shown in Fig. 9. At Terminal R, the effect of the transformer caused the arrival time of the initial TW to not be identified by the UHS relay, making the automatic calculation of the DETWFL results by the relays unavailable. Therefore, the cursor at Terminal R in Fig. 9 that is associated with the t_R time stamp is automatically placed by the Bewley Diagram application. The software calculates this placement based on the t_L time stamp and fault location reported from one of the other available methods in the UHS relay at Terminal L. The figure shows that using two pinned cursors corresponding to t_L and t_R produces a calculated fault location of 34.076 mi (54.840 km) from Terminal L, which differs from the location reported by the line crew by 0.525 mi (2,772 ft; 845 m).

Because the line is terminated at a transformer at Terminal R, the peaks of the measured TWs at this terminal are less distinct—they appear more rounded and elongated. Because the peaks are not well-defined, there may be ambiguity when manually aligning cursors on the Bewley diagram to identify the TW peaks, which may be a source of error in the calculated fault location. Additional error may be introduced by the time-stamping algorithm. Although this algorithm uses interpolation to obtain TW time stamps with submicrosecond accuracy from the individual sample points, it can be adversely affected by TW shape distortions.

In Fig. 10, an additional (third) time cursor is pinned to the Bewley diagram that corresponds to the TW that arrived at Terminal L at time t_{LL}. Pinning the third time cursor allows a new *TWLPT* value of 402.00 μs to be calculated. The new

calculated fault location is 34.116 mi (54.904 km) from Terminal L, which differs from the fault location reported by the line crew by 0.485 mi (2,561 ft; 781 m). Fig. 10 also shows there is misalignment in some of the subsequent TWs that arrive at Terminal L, such as the one corresponding to arrival time t_{RL}.

In Fig. 11, an additional (fourth) time cursor is pinned to the Bewley diagram that corresponds to the TW arriving at Terminal L at time t_{RL}. As explained in Appendix B, pinning four time cursors allows the system of equations to solve for *TWLPT* and Δ. In this case, *TWLPT* is modified to be 398.59 μs, Δ is calculated to be 3.412 μs, and the new calculated fault location is 34.408 mi (55.374 km) from Terminal L. The new result differs from the fault location reported by the line crew by 0.193 mi (1,019 ft; 311 m). Fig. 11 also shows that time cursors corresponding to subsequent TWs arriving at Terminal L are better aligned with the visible peaks in the TW signal. Table I summarizes the results of pinning two, three, and four cursors.

TABLE I.
BEWLEY DIAGRAM RESULTS FOR FAULT
REPORTED BY THE LINE CREW AT 34.601 MI

TW Arrival Times Used for TWFL	FL (mi)	Abs. Error (mi)	*TWLPT*[a] (μs)	Δ[b] (μs)
t_L, t_R	34.076	0.525	395.13	0
t_L, t_R, t_{LL}	34.116	0.485	402.00	0
t_L, t_R, t_{LL}, t_{RL}	34.408	0.193	398.59	3.412

[a] The initial *TWLPT* value is provided by the device settings. Calculation of a new *TWLPT* value requires at least three TW time stamps.
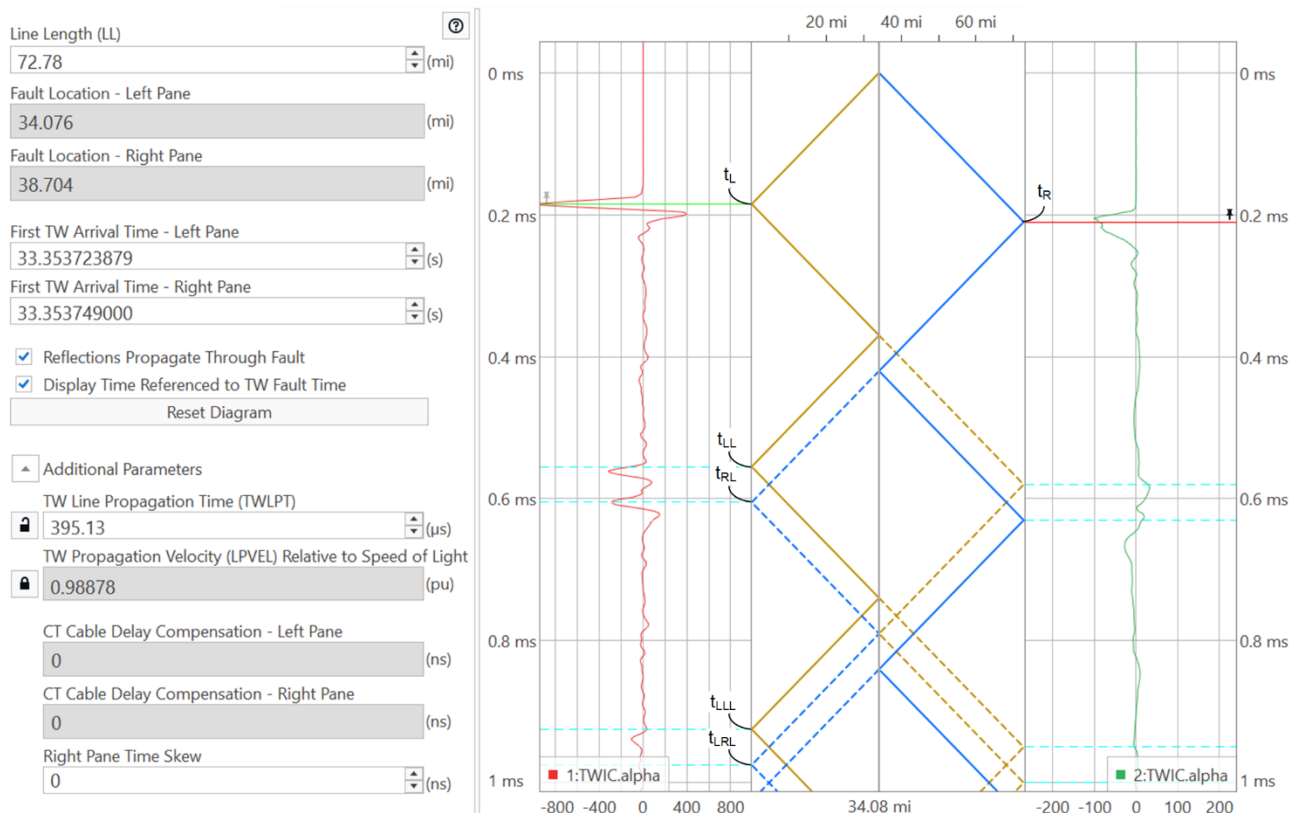[b] Calculation of the skew value requires four TW time stamps.

Fig. 9.   Bewley diagram and DETWFL results obtained by using two TW arrivals (t_L and t_R) to calculate the fault location.
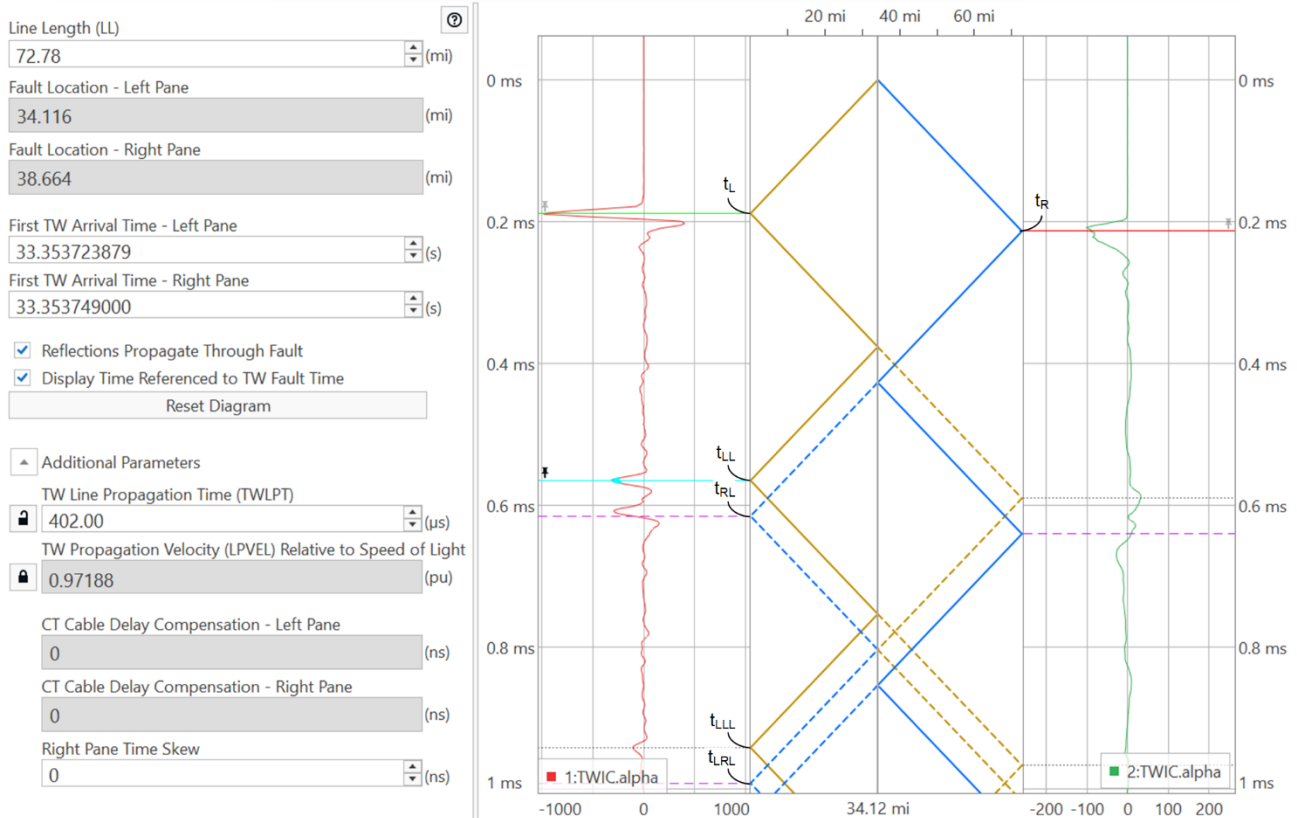
Fig. 10.   Bewley diagram and DETWFL results obtained by using a third TW arrival (t_{LL}) to additionally refine *TWLPT* for improved faut-locating accuracy.
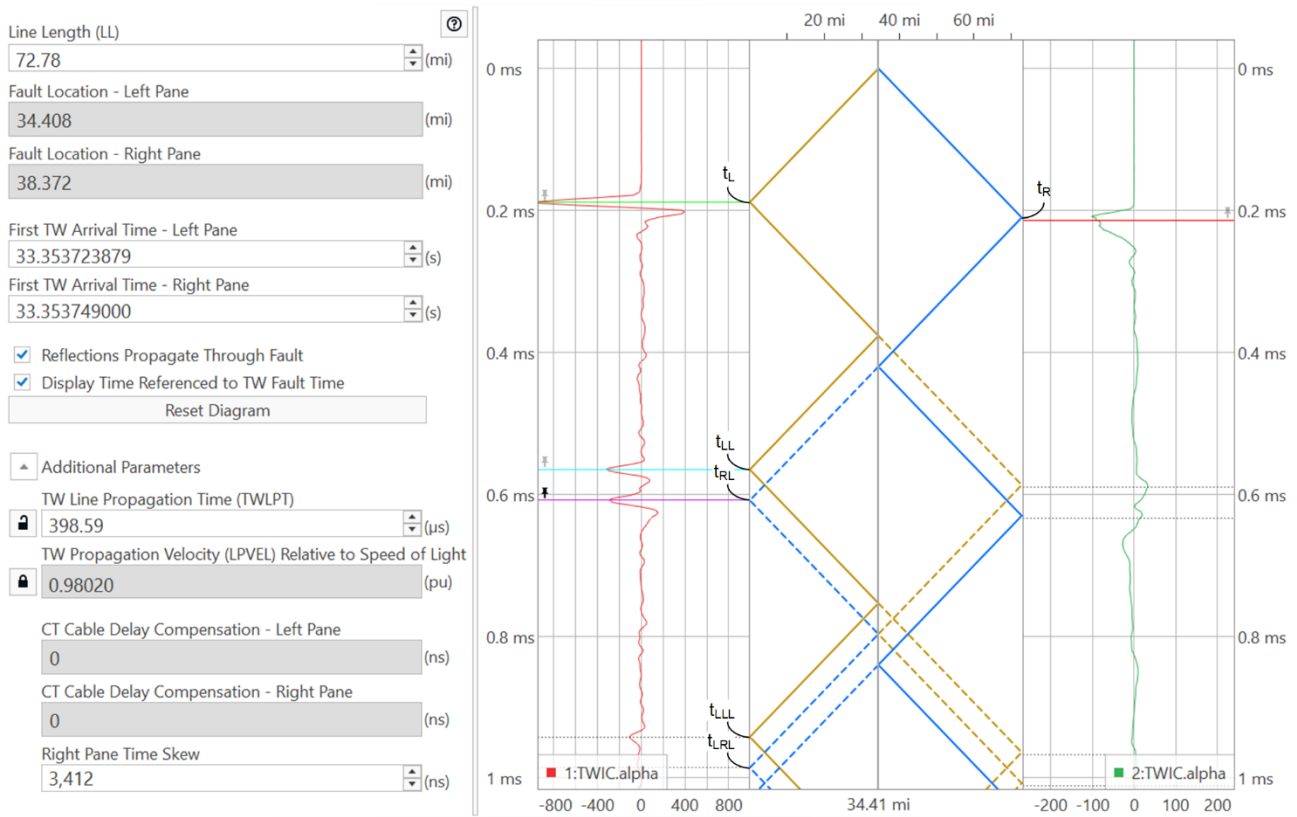

Fig. 11.   Bewley diagram and DETWFL results obtained by using a fourth TW arrival (t_{RL}) to additionally refine Δ to further improve faut-locating accuracy.

Fig. 12 is a zoomed-in view of the initial TWs that arrived at Terminals L and R in Fig. 11. It shows a vertical arrow displayed by the Bewley Diagram application just above the cursor associated with the t_R arrival time. The arrow represents the calculated skew value (Δ) and shows how the TW signal aligns better with the Bewley diagram when compensation for Δ is considered. If the *TWCPT* settings are not set or are suspected to contain errors, the settings engineer may consider using the calculated Δ to set or modify the *TWCPT* settings. Although the *TWCPT* settings were unintentionally set to zero for the example in this section, modifying these settings based on the calculated Δ is not recommended in this case because the TW arrival times at Terminal R were determined by the Bewley Diagram application, rather than the installed devices that use the *TWCPT* settings.
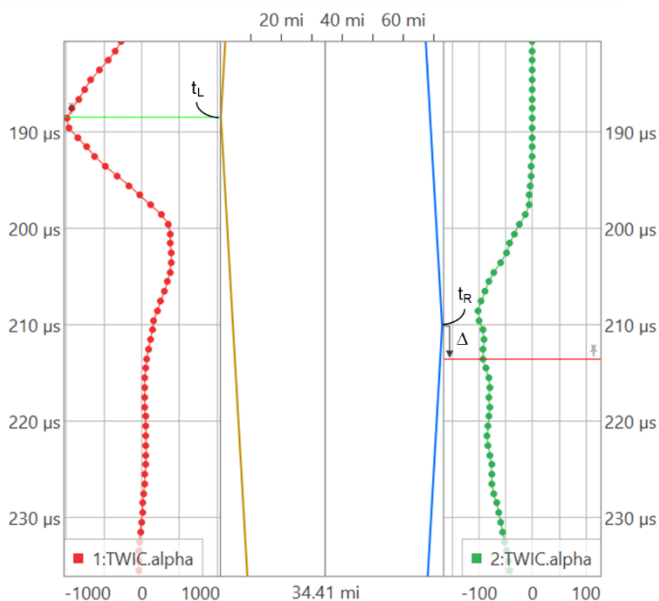

Fig. 12.   Zoomed-in view of t_L and t_R TW arrivals to show the arrow representing the skew (Δ) between the lattice reflection point associated with t_R and the t_R cursor.

V.   CONCLUSION

In this paper, we have shown how the systematic matrix-based method and associated notation regarding TW arrival times provide a flexible and robust method of solving the TWFL equations. Further, allowing flexibility when choosing and pinning cursors to select TWs and including the time skew as a solvable parameter adds additional capability to precisely locate the fault. Incorporating this technique into fault analysis software via a Bewley Diagram application improves operator understanding of the factors affecting the TWFL process and improves the accuracy of the TWFL results.

VI.   APPENDIX A: DERIVATION OF TRAVELING-WAVE-BASED FAULT-LOCATING EQUATIONS FROM A STRUCTURED MATRIX REPRESENTATION

A.   Double-Ended TW-Based Fault Locating by Using Two TW Arrival Times

The general DETWFL equation (7) uses the t_L and t_R TW arrival times to find the per-unit fault location, m.

To derive (7), begin with the definitions of t_L and t_R.

$$t_L = t_0 + m \cdot TWLPT$$
$$t_R = t_0 + (1 - m) \cdot TWLPT$$

Express them in matrix format, $\boldsymbol{Ax} = \boldsymbol{t}$, where $\boldsymbol{A}$ is the TW alignment matrix, $\boldsymbol{x}$ is the 3×1 Bewley lattice parameter vector, and $\boldsymbol{t}$ is the vector of TW arrival times.

$$\begin{bmatrix} 1 & 1 & 0 \\ 1 & -1 & 1 \end{bmatrix} \begin{bmatrix} t_0 \\ m \cdot TWLPT \\ TWLPT \end{bmatrix} = \begin{bmatrix} t_L \\ t_R \end{bmatrix}$$

At this point, *TWLPT* is held constant because we want to use the existing value, so we need to separate this part out.

$$\begin{bmatrix} 1 & 1 \\ 1 & -1 \end{bmatrix} \begin{bmatrix} t_0 \\ m \cdot TWLPT \end{bmatrix} + \begin{bmatrix} 0 \\ TWLPT \end{bmatrix} = \begin{bmatrix} t_L \\ t_R \end{bmatrix}$$

Next, we isolate the part containing the variables we are solving for: t_0 and $m \cdot TWLPT$.

$$\begin{bmatrix} 1 & 1 \\ 1 & -1 \end{bmatrix} \begin{bmatrix} t_0 \\ m \cdot TWLPT \end{bmatrix} = \begin{bmatrix} t_L \\ t_R \end{bmatrix} - \begin{bmatrix} 0 \\ TWLPT \end{bmatrix}$$

Remove the matrix in front of our variables of interest by premultiplying by its inverse, $\boldsymbol{A}^{-1}$. To be invertible, the $\boldsymbol{A}$ matrix must be full rank. To be full rank, the rows must be linearly independent as indicated by a nonzero value when the matrix determinant is calculated [6]. Thus, we confirm that the determinant of $\boldsymbol{A}$ is nonzero ($\det(\boldsymbol{A}) = -2$) before attempting to calculate its inverse.

$$\begin{bmatrix} 1 & 1 \\ 1 & -1 \end{bmatrix}^{-1} \left(\begin{bmatrix} t_L \\ t_R \end{bmatrix} - \begin{bmatrix} 0 \\ TWLPT \end{bmatrix} \right) = \begin{bmatrix} t_0 \\ m \cdot TWLPT \end{bmatrix}$$

$$\frac{1}{2} \begin{bmatrix} 1 & 1 \\ 1 & -1 \end{bmatrix} \left(\begin{bmatrix} t_L \\ t_R \end{bmatrix} - \begin{bmatrix} 0 \\ TWLPT \end{bmatrix} \right) = \begin{bmatrix} t_0 \\ m \cdot TWLPT \end{bmatrix}$$

Simplify:

$$\begin{bmatrix} t_0 \\ m \cdot TWLPT \end{bmatrix} = \frac{1}{2} \begin{bmatrix} t_L + t_R - TWLPT \\ t_L - t_R + TWLPT \end{bmatrix}$$

Solve for m:

$$m \cdot TWLPT = \frac{1}{2}(t_L - t_R + TWLPT)$$

$$m = \frac{1}{2} \left(\frac{t_L - t_R + TWLPT}{TWLPT} \right)$$

$$m = \frac{1}{2} \left(1 + \frac{t_L - t_R}{TWLPT} \right)$$

B. Single-Ended TW-Based Fault Locating by Using Two TW Arrival Times

The general SETWFL equation (11) uses the t_L and t_{LL} TW arrival times to find the per-unit fault location, m.

To derive (11), begin with the definitions of tL and tLL.

$$t_L = t_0 + m \cdot TWLPT$$

$$t_{LL} = t_0 + 3m \cdot TWLPT$$

Express them in matrix format, $Ax = t$, where A is the TW alignment matrix, x is the 3×1 Bewley lattice parameter vector, and t is the vector of TW arrival times.

$$\begin{bmatrix} 1 & 1 & 0 \\ 1 & 3 & 0 \end{bmatrix} \begin{bmatrix} t_0 \\ m \cdot TWLPT \\ TWLPT \end{bmatrix} = \begin{bmatrix} t_L \\ t_{LL} \end{bmatrix}$$

Because $TWLPT$ is multiplied by 0, we can remove it from the equation.

$$\begin{bmatrix} 1 & 1 \\ 1 & 3 \end{bmatrix} \begin{bmatrix} t_0 \\ m \cdot TWLPT \end{bmatrix} = \begin{bmatrix} t_L \\ t_{LL} \end{bmatrix}$$

Remove the matrix in front of our variables of interest by premultiplying by its inverse, A^{-1}. To be invertible, the A matrix must be full rank; thus, we confirm that the determinant of A is nonzero ($\det(A) = 2$) before attempting to calculate its inverse.

$$\begin{bmatrix} t_0 \\ m \cdot TWLPT \end{bmatrix} = \begin{bmatrix} 1 & 1 \\ 1 & 3 \end{bmatrix}^{-1} \begin{bmatrix} t_L \\ t_{LL} \end{bmatrix}$$

$$\begin{bmatrix} t_0 \\ m \cdot TWLPT \end{bmatrix} = \frac{1}{2} \begin{bmatrix} 3 & -1 \\ -1 & 1 \end{bmatrix} \begin{bmatrix} t_L \\ t_{LL} \end{bmatrix}$$

Simplify:

$$\begin{bmatrix} t_0 \\ m \cdot TWLPT \end{bmatrix} = \frac{1}{2} \begin{bmatrix} 3t_L - t_{LL} \\ -t_L + t_{LL} \end{bmatrix}$$

Solve for m:

$$m \cdot TWLPT = \frac{1}{2}(t_{LL} - t_L)$$

$$m = \frac{1}{2}\left(\frac{t_{LL} - t_L}{TWLPT}\right)$$

VII. APPENDIX B: SOLVING THE FOUR-DIMENSIONAL TRAVELING-WAVE-BASED FAULT-LOCATING EQUATIONS FOR 1, 2, 3, AND 4 DEGREES OF FREEDOM

The process of solving the TWFL matrix equation in the Bewley Diagram application is performed using the following method. The equation is expressed as $Ax = t$, where A is the TW alignment matrix, x is the 4×1 Bewley lattice parameter vector, and t is the vector of TW arrival times. The method is different depending on how many TW arrival times are included. A TW arrival time is included if its position is fixed (i.e., if the corresponding cursor is pinned in the application) or if the TW arrival is associated with the cursor that is being manipulated by the operator. The positions of all other TW arrival times are dynamically calculated from the parameter values that result from the calculations below. The A matrix is partitioned into a square: A_V corresponding to the variable portion of x (x_V), and A_F corresponding to the fixed portion of x (x_F).

$$[A][x] = [A_V \quad A_F] \begin{bmatrix} x_V \\ x_F \end{bmatrix}$$

The partitioning depends on the size of the original A matrix, as shown later in this appendix. For example, if the dimensions of A are 1×4, to make A_V square, it must be 1×1, leaving A_F to be 1×3.

The procedures below include inverting A_F. A matrix is only invertible if it is full rank (i.e., its rows are linearly independent as indicated by a nonzero determinant) [6]. In the Bewley Diagram application, a cursor can only be manipulated and/or pinned if adding that row to the existing A matrix will result in a new square A_V matrix with a nonzero determinant. Mathematically, a new row of A may only be included if it adds information that enables solving for the next element of x.

A. One Degree of Freedom

A one-degree-of-freedom scenario occurs when only one TW arrival time is included in the calculation. This occurs if the operator is manipulating a cursor and no other cursors are pinned or if only one cursor is pinned and the operator is presently manipulating that cursor. In this case, t_0 is our variable of interest and all other variables ($m \cdot TWLPT$, $TWLPT$, and Δ) remain constant.

The single TW arrival time is shown as t_1 in (B.1). The A matrix that multiplies the Bewley parameters is the row of (16a) or (16b) corresponding to t_1.

Begin with the equation for t_1. The dimensions of the A matrix are 1×4.

$$[A_{11} \quad A_{12} \quad A_{13} \quad A_{14}] \begin{bmatrix} t_0 \\ m \cdot TWLPT \\ TWLPT \\ \Delta \end{bmatrix} = [t_1] \quad (B.1)$$

Isolate the parameter of interest by separating Ax into $A_V x_V + A_F x_F$.

$$[A_{11}][t_0] + [A_{12} \quad A_{13} \quad A_{14}] \begin{bmatrix} m \cdot TWLPT \\ TWLPT \\ \Delta \end{bmatrix} = [t_1]$$

Isolate $A_V x_V$ (i.e., the parameter of interest) to the left side of the equation.

$$[A_{11}][t_0] = [t_1] - [A_{12} \quad A_{13} \quad A_{14}] \begin{bmatrix} m \cdot TWLPT \\ TWLPT \\ \Delta \end{bmatrix}$$

Solve for x_V by premultiplying both sides by the inverse of the A_V matrix, A_V^{-1}.

$$[t_0] = [A_{11}]^{-1}$$

$$\left([t_1] - [A_{12} \quad A_{13} \quad A_{14}] \begin{bmatrix} m \cdot TWLPT \\ TWLPT \\ \Delta \end{bmatrix}\right)$$

B. Two Degrees of Freedom

A two-degree-of-freedom scenario occurs when only two TW arrival times are included in the calculation. This occurs if the operator is manipulating a cursor and one other cursor is pinned or if only two cursors are pinned and the operator is

presently manipulating one of the pinned cursors. In this case, t_0 and $m \cdot TWLPT$ are our variables of interest and all other variables ($TWLPT$ and Δ) remain constant.

The two TW arrival times are shown as t_1 and t_2 in (B.2). The A matrix that multiplies the Bewley parameters comprises two rows corresponding to t_1 and t_2 taken from (16a) or (16b).

The dimensions of the A matrix for t_1 and t_2 are 2×4.

$$\begin{bmatrix} A_{11} & A_{12} & A_{13} & A_{14} \\ A_{21} & A_{22} & A_{23} & A_{24} \end{bmatrix} \begin{bmatrix} t_0 \\ m \cdot TWLPT \\ TWLPT \\ \Delta \end{bmatrix} = \begin{bmatrix} t_1 \\ t_2 \end{bmatrix} \quad \text{(B.2)}$$

Isolate the parameters of interest by separating the A matrix into a square 2×2 matrix (A_V) times our parameters of interest (x_V) and a separate matrix (A_F) times the constant parameters (x_F).

$$\begin{bmatrix} A_{11} & A_{12} \\ A_{21} & A_{22} \end{bmatrix} \begin{bmatrix} t_0 \\ m \cdot TWLPT \end{bmatrix} + \begin{bmatrix} A_{13} & A_{14} \\ A_{23} & A_{24} \end{bmatrix} \begin{bmatrix} TWLPT \\ \Delta \end{bmatrix} = \begin{bmatrix} t_1 \\ t_2 \end{bmatrix}$$

Isolate the parameters of interest to the left side of the equation.

$$\begin{bmatrix} A_{11} & A_{12} \\ A_{21} & A_{22} \end{bmatrix} \begin{bmatrix} t_0 \\ m \cdot TWLPT \end{bmatrix} = \begin{bmatrix} t_1 \\ t_2 \end{bmatrix} - \begin{bmatrix} A_{13} & A_{14} \\ A_{23} & A_{24} \end{bmatrix} \begin{bmatrix} TWLPT \\ \Delta \end{bmatrix}$$

Cancel out the square A matrix by premultiplying both sides by its inverse, A_V^{-1}.

$$\begin{bmatrix} t_0 \\ m \cdot TWLPT \end{bmatrix} = $$
$$\begin{bmatrix} A_{11} & A_{12} \\ A_{21} & A_{22} \end{bmatrix}^{-1} \left(\begin{bmatrix} t_1 \\ t_2 \end{bmatrix} - \begin{bmatrix} A_{13} & A_{14} \\ A_{23} & A_{24} \end{bmatrix} \begin{bmatrix} TWLPT \\ \Delta \end{bmatrix} \right)$$

C. Three Degrees of Freedom

A three-degree-of-freedom scenario occurs when three TW arrival times are included in the calculation. This occurs if the operator is manipulating a cursor and two other cursors are pinned or if three cursors are pinned and the operator is presently manipulating one of the pinned cursors. In this case, t_0, $m \cdot TWLPT$, and $TWLPT$ are our variables of interest and Δ remains constant.

The three TW arrival times are shown as t_1, t_2, and t_3 in (B.3). The A matrix that multiplies the Bewley parameters comprises three rows corresponding to t_1, t_2, and t_3 taken from (16a) or (16b).

The dimensions of the A matrix for t_1, t_2, and t_3 are 3×4.

$$\begin{bmatrix} A_{11} & A_{12} & A_{13} & A_{14} \\ A_{21} & A_{22} & A_{23} & A_{24} \\ A_{31} & A_{32} & A_{33} & A_{34} \end{bmatrix} \begin{bmatrix} t_0 \\ m \cdot TWLPT \\ TWLPT \\ \Delta \end{bmatrix} = \begin{bmatrix} t_1 \\ t_2 \\ t_3 \end{bmatrix} \quad \text{(B.3)}$$

Isolate the parameters of interest by separating the A matrix into a square 3×3 matrix (A_V) times our parameters of interest (x_V) and a separate matrix (A_F) times the constant parameter (x_F).

$$\begin{bmatrix} A_{11} & A_{12} & A_{13} \\ A_{21} & A_{22} & A_{23} \\ A_{31} & A_{32} & A_{33} \end{bmatrix} \begin{bmatrix} t_0 \\ m \cdot TWLPT \\ TWLPT \end{bmatrix} + \begin{bmatrix} A_{14} \\ A_{24} \\ A_{34} \end{bmatrix} [\Delta] = \begin{bmatrix} t_1 \\ t_2 \\ t_3 \end{bmatrix}$$

Isolate the parameters of interest to the left side of the equation.

$$\begin{bmatrix} A_{11} & A_{12} & A_{13} \\ A_{21} & A_{22} & A_{23} \\ A_{31} & A_{32} & A_{33} \end{bmatrix} \begin{bmatrix} t_0 \\ m \cdot TWLPT \\ TWLPT \end{bmatrix} = \begin{bmatrix} t_1 \\ t_2 \\ t_3 \end{bmatrix} - \begin{bmatrix} A_{14} \\ A_{24} \\ A_{34} \end{bmatrix} [\Delta]$$

Cancel out the square A matrix by premultiplying both sides by its inverse, A_V^{-1}.

$$\begin{bmatrix} t_0 \\ m \cdot TWLPT \\ TWLPT \end{bmatrix} = $$
$$\begin{bmatrix} A_{11} & A_{12} & A_{13} \\ A_{21} & A_{22} & A_{23} \\ A_{31} & A_{32} & A_{33} \end{bmatrix}^{-1} \left(\begin{bmatrix} t_1 \\ t_2 \\ t_3 \end{bmatrix} - \begin{bmatrix} A_{14} \\ A_{24} \\ A_{34} \end{bmatrix} [\Delta] \right)$$

D. Four Degrees of Freedom

A four-degree-of-freedom scenario occurs when four TW arrival times are included in the calculation. This occurs if the operator is manipulating a cursor and three other cursors are pinned or if four cursors are pinned and the operator is presently manipulating one of the pinned cursors. In this case, t_0, $m \cdot TWLPT$, $TWLPT$, and Δ are our parameters of interest and none remain constant.

The four TW arrival times are shown as t_1, t_2, t_3, and t_4 in (B.4). The A matrix that multiplies the Bewley parameters comprises four rows corresponding to t_1, t_2, t_3, and t_4 taken from (16a) or (16b).

The dimensions of the A matrix for t_1, t_2, t_3, and t_4 are 4×4; thus, $A_V = A$ and $x_V = x$. A_F and x_F are both empty.

$$\begin{bmatrix} A_{11} & A_{12} & A_{13} & A_{14} \\ A_{21} & A_{22} & A_{23} & A_{24} \\ A_{31} & A_{32} & A_{33} & A_{34} \\ A_{41} & A_{42} & A_{43} & A_{44} \end{bmatrix} \begin{bmatrix} t_0 \\ m \cdot TWLPT \\ TWLPT \\ \Delta \end{bmatrix} = \begin{bmatrix} t_1 \\ t_2 \\ t_3 \\ t_4 \end{bmatrix} \quad \text{(B.4)}$$

Cancel out the square A matrix by premultiplying both sides by its inverse, A^{-1}.

$$\begin{bmatrix} t_0 \\ m \cdot TWLPT \\ TWLPT \\ \Delta \end{bmatrix} = \begin{bmatrix} A_{11} & A_{12} & A_{13} & A_{14} \\ A_{21} & A_{22} & A_{23} & A_{24} \\ A_{31} & A_{32} & A_{33} & A_{34} \\ A_{41} & A_{42} & A_{43} & A_{44} \end{bmatrix}^{-1} \begin{bmatrix} t_1 \\ t_2 \\ t_3 \\ t_4 \end{bmatrix}$$

VIII. Acknowledgment

IX. References

[1] E. O. Schweitzer, III, A. Guzmán, M. V. Mynam, V. Skendzic, B. Kasztenny, and S. Marx, "Locating Faults by the Traveling Waves They Launch," proceedings of the 40th Annual Western Protective Relay Conference, Spokane, WA, October 2013.

[2] A. Guzmán, B. Kasztenny, Y. Tong, and M. V. Mynam, "Accurate and Economical Traveling-Wave Fault Locating Without Communications," proceedings of the 44th Annual Western Protective Relay Conference, Spokane, WA, October 2017.

[3] B. Kasztenny and V. Mynam, "Line Length and Fault Distance Considerations in Travelling-Wave Protection and Fault-Locating Applications," May 2021. Available: selinc.com.

[4] L. V. Bewley, "Traveling Waves on Transmission Systems," proceedings of the Winter Convention of the American Institute of Electrical Engineers, New York, NY, January 1931, pp. 532–550.

[5] L. V. Bewley, *Traveling Wave on Transmission Systems*, 2nd ed., Dover Publications, New York, NY, 1963.

[6] J. Hefferon, *Linear Algebra*, 4th ed. Available: https://hefferon.net/linearalgebra/.

[7] B. Kasztenny, A. Guzmán, M. V. Mynam, and T. Joshi, "Locating Faults Before the Breaker Opens – Adaptive Autoreclosing Based on the Location of the Fault," proceedings of the 44th Annual Western Protective Relay Conference, Spokane, WA, October 2017.

[8] D. L. Cortón, J. V. Melado, J. Cruz, R. Kirby, Y. Z. Korkmaz, G. Patti, and G. Smelich, "Double-Ended Traveling-Wave Fault Locating Without Relay-to-Relay Communications," proceedings of the 74th Annual Conference for Protective Relay Engineers, College Station, TX, March 2021.

[9] SEL-5601-2 SYNCHROWAVE Event Software Instruction Manual. Available: selinc.com.

[10] D. Halliday and R. Resnick, *Physics, Parts 1 & 2, Combined Edition*, John Wiley & Sons, Inc., New York, NY, 1966.

[11] L. L. Scharf, *Statistical Signal Processing: Detection, Estimation, and Time Series Analysis*, Pearson publishing, 1991.

X. BIOGRAPHIES

Stephen Marx received his BSEE from the University of Utah in 1988. He joined Bonneville Power Administration (BPA) in 1988 where he is presently the District Engineer in Idaho Falls, Idaho. He has over 34 years of experience in power system protection and metering and has been a lecturer at the Hands-On Relay School in the state of Washington since 2007. He has authored and coauthored several technical papers. He is a registered professional engineer in the state of Oregon and a member of the IEEE.

Ellery Blood is a principal engineer at Schweitzer Engineering Laboratories, Inc. (SEL). He designs software, performs control research, and holds multiple patents. Before joining SEL, Ellery taught systems engineering as an assistant professor at the U.S. Naval Academy. He is an active Naval Reservist supporting the Office of Naval Research. He holds both a PhD and a master's degree in electrical and computer engineering from Carnegie Mellon University. He also earned a master's degree in mechanical engineering from the Naval Postgraduate School and a bachelor's degree in computer and systems engineering from Rensselaer Polytechnic Institute. Ellery is a Senior Member of the IEEE.

Greg Smelich earned a BS in mathematical science and an MS in electrical engineering in 2008 and 2011, respectively, from Montana Tech of the University of Montana. Greg then began his career at Schweitzer Engineering Laboratories, Inc. (SEL) as a protection application engineer in the sales and customer service division. In 2016, he transitioned to the research and development division as a product engineer where he now helps guide product development and provides training and technical support primarily related to time-domain technology. He has coauthored several technical papers and application guides on various topics related to power system protection and fault locating. He has been a certified SEL University instructor since 2011, an adjunct professor in the electrical engineering department at Montana Tech since 2017, and an international technical committee member of the CIGRE Canada Conference since 2018. Greg is an active member of the IEEE and a registered professional engineer in the state of Washington.